Chaos, Solitons and Fractals 142 (2021) 110431

Contents lists available at ScienceDirect

Chaos, Solitons and Fractals

Nonlinear Science, and Nonequilibrium and Complex Phenomena

journal homepage: www.elsevier.com/locate/chaos

Dynamics of epidemics: Impact of easing restrictions and control of infection spread

Silvio L.T. de Souza[a,*], Antonio M. Batista[b,c], Iberê L. Caldas[c], Kelly C. Iarosz[c,d,e], José D. Szezech Jr[b]

[a] Federal University of São João del-Rei, Campus Centro-Oeste, Divinópolis, MG 35501-296, Brazil
[b] Department of Mathematics and Statistics, State University of Ponta Grossa, Ponta Grossa, PR 84030-900, Brazil
[c] Institute of Physics, University of São Paulo, São Paulo, SP 05508-090, Brazil
[d] Faculdade de Telêmaco Borba, FATEB, Telêmaco Borba, PR 84266-010, Brazil
[e] Graduate Program in Chemical Engineering Federal Technological University of Paraná, Ponta Grossa, PR 84016-210, Brazil

ARTICLE INFO

Article history:
Received 15 July 2020
Revised 19 October 2020
Accepted 2 November 2020
Available online 12 November 2020

Keywords:
COVID-19
SEIR model
Easing restrictions
Spikes of infections
Control of infection spread

ABSTRACT

During an infectious disease outbreak, mathematical models and computational simulations are essential tools to characterize the epidemic dynamics and aid in design public health policies. Using these tools, we provide an overview of the possible scenarios for the COVID-19 pandemic in the phase of easing restrictions used to reopen the economy and society. To investigate the dynamics of this outbreak, we consider a deterministic compartmental model (SEIR model) with an additional parameter to simulate the restrictions. In general, as a consequence of easing restrictions, we obtain scenarios characterized by high spikes of infections indicating significant acceleration of the spreading disease. Finally, we show how such undesirable scenarios could be avoided by a control strategy of successive partial easing restrictions, namely, we tailor a successive sequence of the additional parameter to prevent spikes in phases of low rate of transmissibility.

1. Introduction

The emergence of infectious diseases with epidemic potential requires massive interdisciplinary efforts to understand and develop measures to prevent or, at least, mitigate outbreaks [1,2]. In this context, mathematical models have played an important role in understanding the dynamics of infectious diseases and in designing health policy strategies [3–7]. In fact, these models have been used extensively to investigate different types of infection dynamics such as influenza A [8], Zika [9], Ebola [10], SARS [11,12], MERS [13,14], and, more recently, COVID-19 [15–20].

During a pandemic like COVID-19, besides the important work of forecasting [21] and evaluating public health strategies [22], the impact of easing containment measures should be carefully evaluated to avoid drastic spikes in infections and, consequently, reimpose heavy social and economic restrictions.

In this work, we investigate possible outcomes for the COVID-19 outbreak in the phase of lifting containment measures. For numerical studies, we consider the SEIR model (Susceptible - Exposed - Infected - Removed) with an additional parameter to simulate the restrictions. We also provide a control strategy to prevent spikes in infections by easing restrictions. In other words, our main purpose is to cast further light on the dynamical scenarios for the course of the COVID-19 pandemic in the context of reopening the economy and society.

This paper is organized as follows: In Section 2, we introduce the SEIR model with an additional control parameter providing an initial overview of the epidemic behavior. In Section 3, we investigate the impact of easing restrictions on the infection dynamics. In Section 4, we explore a control strategy to avoid spikes and reduce the transmission rate. The last section contains our main remarks.

2. Mathematical modeling of epidemics

Compartmental models derived from classical SEIR model have been used extensively to forecast the evolution of the COVID-19 outbreak [23–27]. The main idea to introduce these type of models is to divide the population into a set of distinct classes. For example, individuals for the basic SEIR model are separated into four compartments: susceptible (S), exposed (E), infected (I), and recovered or removed (R) classes.

For numerical simulation, we consider the SEIR model with additional control term $(1-\sigma)$ as used by Boldog and collaborators

* Corresponding author.
E-mail address: thomaz@ufsj.edu.br (S.L.T. de Souza).

https://doi.org/10.1016/j.chaos.2020.110431
0960-0779/

[28]. Thus, the compartmental deterministic model is given by the set of ordinary differential equations:

$$\frac{dS}{dt} = -\frac{\beta}{N}SI(1-\sigma), \tag{1}$$

$$\frac{dE}{dt} = \frac{\beta}{N}SI(1-\sigma) - \omega E, \tag{2}$$

$$\frac{dI}{dt} = \omega E - \gamma I, \tag{3}$$

$$\frac{dR}{dt} = \gamma I, \tag{4}$$

where $\beta \equiv R_0/T_{inf}$ is the transmission rate, $\omega \equiv 1/T_{inc}$ is the transition rate from E to I, $\gamma \equiv 1/T_{inf}$ is the transition rate from I to R, and $N = S + E + I + R$ is the total population for incubation period T_{inc}, infectious period T_{inf}, and basic reproductive number R_0 with σ on the interval [0,1]. In this case, the effective reproductive number is given by $R_t = R_0(1-\sigma)S/N$. Thus, in case of $R_0 = 3$ the parameter σ must be 2/3 or greater ($2/3 \leq \sigma \leq 1$) in order to suppress the epidemic spreading [29]. Additionally, the parameter σ describes the intensity of restrictions associated with control policies to reduce the infection spread. For example, this parameter can represent the fraction of the infected individuals subjected to isolation.

Based on recent study on dynamics of transmission and control of COVID-19 [30], we consider the control parameters $T_{inc} = 5.2$ days, $T_{inf} = 2.9$ days and $R_0 = 3$. The basic reproductive number R_0 depends on various factors, such as the probability of infection and the rate of contacts. In Wuhan during January of 2020, the median R_0 values ranged from 1.6 to 2.6 [30]. At the beginning of the outbreak of COVID-19, the European Union presented $R_0 = 4.22 \pm 1.69$ [31]. Therefore, R_0 equal to 3 is inside the interval of values observed in many places. For numerical investigation we use $I_0 = R_0 = 0$, $E_0 = 1$ and $S_0 = N - 1$ as initial conditions, fixing the population at $N = 1000$ (normalized to 1000). In order to evaluate the number of individuals S, E, I, and R for a real population of people (P), we have to multiply these dynamical variables by $P/1000$.

Fig. 1 a displays a typical time-series picture of the SEIR model in terms of the dynamical variables S (blue line), E (yellow line), I (red line), and R (green line) for $\sigma = 0.0$. In Fig. 1b, taking into account σ to reduce the spread of the epidemic, we provide a qualitatively robust verification of the curve phenomenon flattening, whose signature is indicated by attenuated and delayed peaks of infections. In other words, increasing the σ value, the amplitude of peaks decreases considerably from 105.5 infections ($\sigma = 0$, red line) to 77.4 ($\sigma = 0.2$, blue line), 42.2 ($\sigma = 0.4$, indigo line), 22.7 ($\sigma = 0.5$, green line), and 5.6 ($\sigma = 0.6$, black line) infections per 1000. Considering $E_0 = 1$, the peak of I for $N = 10^6$ is obtained later than the one for $N = 10^3$. The results for $N = 10^3$ and $N = 10^6$ are the same when it is considered $E_0 = 1$ and $E_0 = 10^3$, respectively.

In fact, for practical purposes flattening the curve is a desirable outcome associated with mitigation strategies, such as physical distancing, mobility restriction, isolation of infected people, and so on. Despite the importance of restriction measures, during the epidemic process easing restrictions will be certainly considered as planning procedures to reopen the economy and society. To evaluate the impact of these procedures we explore the dynamics of the contagious curve by varying the parameter σ.

3. Impact of restriction measures

Initially, we report possible outcomes as a result of moving to a situation without any restrictions (old normal life) modeled by applying $\sigma = 0$. In Fig. 2a, a soft flattened curve in black ($\sigma = 0.4$) is driven to an amplified peak in red ($\sigma = 0.0$) or a moderated curve in blue ($\sigma = 0.0$), depending on the intervention moment. This unrealistic scenario illustrates a biased view that getting past peak (curve in black) the epidemic is over (curve in blue) and the public health interventions can be totally relaxed. In general, the second peak is much more prominent, whose amplification is associated with the number of susceptible people. For instance, Fig. 2b shows a more realistic case for a flattened curve in black ($\sigma = 0.57$) driven to an amplified second peak in blue ($\sigma = 0.0$). In case of the effectiveness of containment measures, removing all restrictions, independently of the moment, results in a drastic spike in the number of infections, as shown in Fig. 2c. As an additional possibility, Fig. 2 d presents a typical case of second wave (in blue), which is characterized by a resurgence of infection after several days of reporting few cases.

To provide a better overview of the effects resulting from removing all restrictions, we investigate the epidemic model using two-dimensional diagrams. (Such diagrams have been used extensively to characterize the dynamics of the diverse chaotic oscillators in two-parameter space [32–37].) In Fig. 3a–d we display the diagrams in terms of time and the parameter σ for a grid of 1000 × 1000 cells. In the same manner as designed in Fig. 2a–d, the simulation is performed for an epidemic curve by applying a particular σ (ranging from 0.4 to 0.7) at the very beginning and turning off σ (setting $\sigma = 0$) at a specific time (ranging from 0 to 400 days).

Fig. 3 a shows the resulting responses, whose color is allocated according to the value of peaks. The crosses (in white and blue)

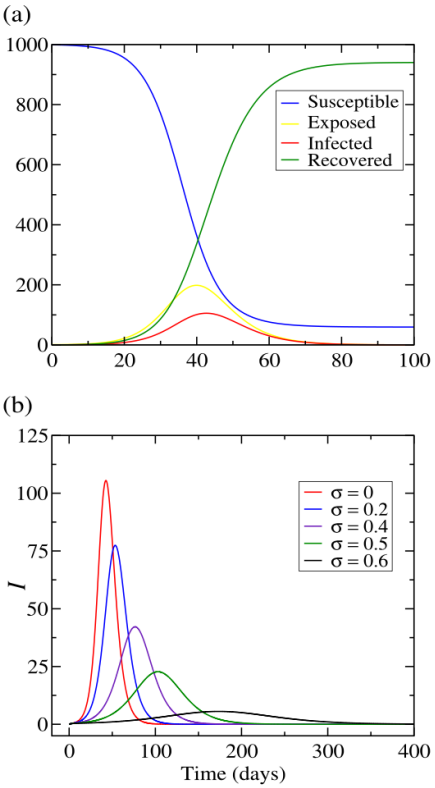

Fig. 1. (a) Time-series of S (blue line), E (yellow line), I (red line), and R (green line) for $\beta = 3/2.9$, $\omega = 1/5.2$, $\gamma = 1/2.9$, and $\sigma = 0$. (b) Time-series of I for $\sigma = 0$ (red line), $\sigma = 0.2$ (blue line), $\sigma = 0.4$ (indigo line), $\sigma = 0.5$ (green line), and $\sigma = 0.6$ (black line). (For interpretation of the references to colour in this figure legend, the reader is referred to the web version of this article.)

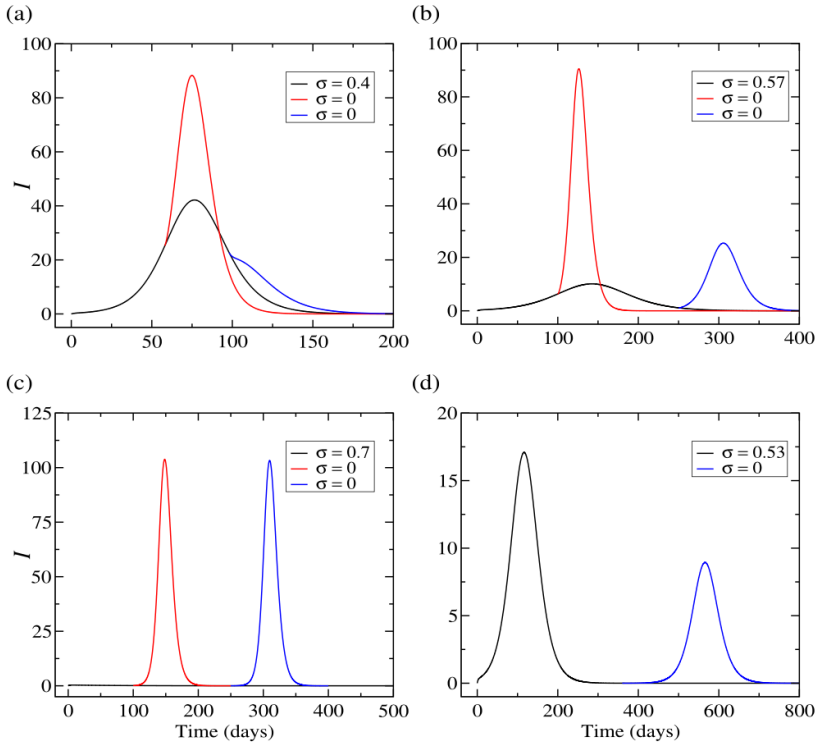

Fig. 2. Time-series of I showing the effect of relaxing totally the restrictions ($\sigma = 0$, red and blue lines) for (a) $\sigma = 0.40$, (b) $\sigma = 0.57$, (c) $\sigma = 0.70$, and (d) $\sigma = 0.53$. (For interpretation of the references to colour in this figure legend, the reader is referred to the web version of this article.)

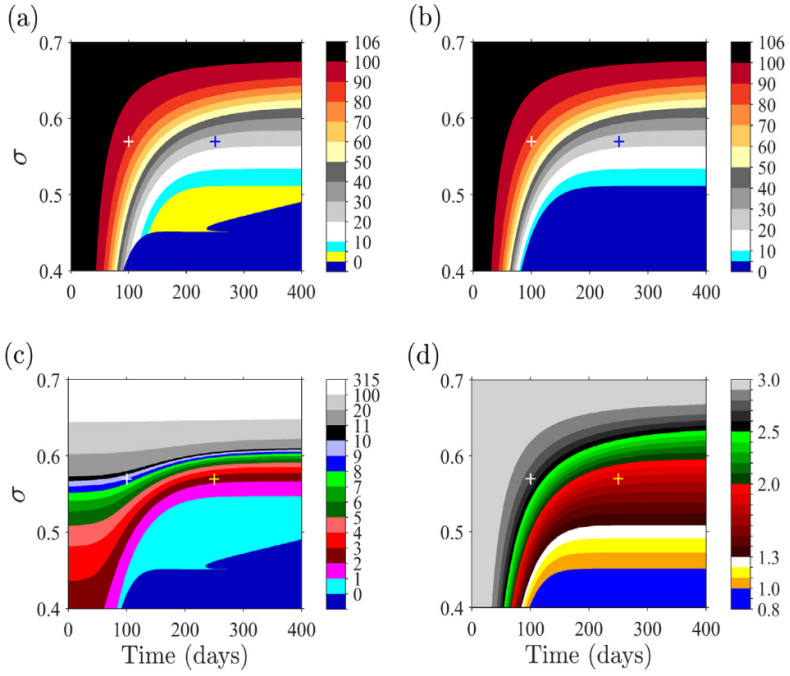

Fig. 3. Two-dimensional diagram of σ *versus* Time (moment) showing (a) the value of peaks after removing restrictions; (b) the difference between the numbers of infections at the peak and the moment of relaxing restriction; (c) the ratio between the new peak value and the flattened curve peak; (d) the value of the effective reproductive number ($R_t = R_0 S/N$) at the moment of relaxing restriction. The crosses indicate the behavior shown in Fig. 2b.

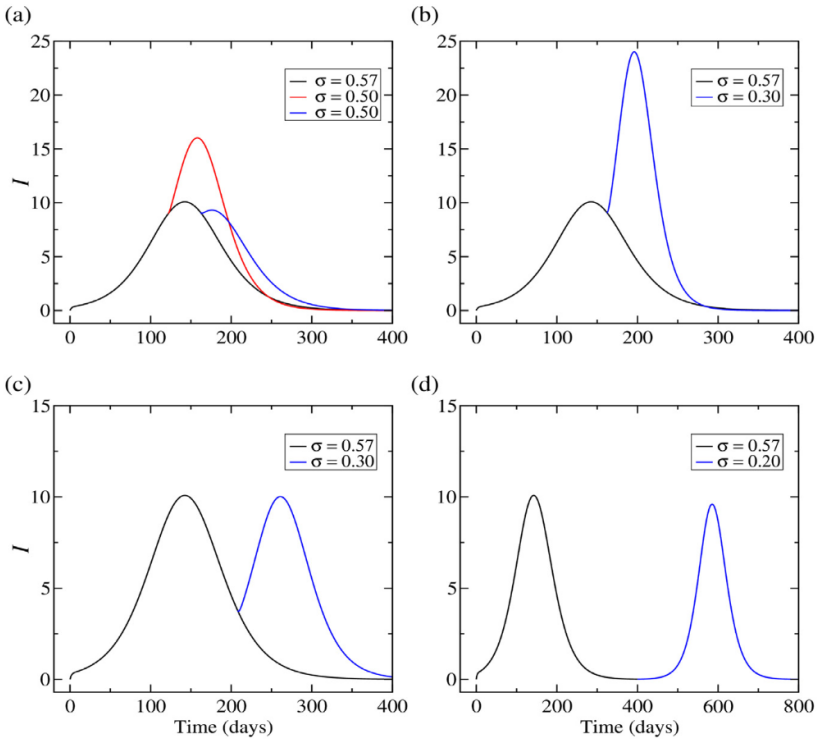

Fig. 4. Time-series of I showing the effect of relaxing the restrictions from $\sigma = 0.57$ (black line) to (a) $\sigma = 0.50$ (red and blue lines), (b) $\sigma = 0.30$ (blue line), (c) $\sigma = 0.30$ (blue line), and (d) $\sigma = 0.20$ (blue line). (For interpretation of the references to colour in this figure legend, the reader is referred to the web version of this article.)

indicate the behavior shown in Fig. 2b and the area in blue corresponds to the same attenuated curve behavior shown in Fig. 2a. Fig. 3b presents another display showing colors according to the difference between numbers of infections at the peak and at the initial suppression of restriction moment ($\sigma = 0$). Besides, we consider two more possibilities to evaluate the outcomes by using the ratio between the new peak value and the flattened curve peak and using the effective reproductive number ($R_t = R_0 S/N$) as shown in Fig. 3c and d, respectively. Comparing Fig. 3b and d we verify that the size of peaks depends directly on effective reproductive numbers (susceptible people). Moreover, we also identify in Fig. 3a and c that the size of peaks for a specific time is subject to the hardiness of a priory restrictions. In other words, the new peaks increase according to the intensity level of the initial σ. In summary, any scenario described by a reasonable level of restrictions moving to total suppression restrictions results in a spike denoting the acceleration of spreading.

Fig. 4 a presents the effect of a partial relaxing intervention, changing σ from 0.57 (in black) to 0.50 (in red and in blue). In this case, it is remarkable the difference between applying the same intensity of intervention at before and after passing the peak of the outbreak. Before passing the peak moment any easing restriction (a small change in σ) results in a significantly different outcome composed of a high amplitude spike. In addition, as shown in Fig. 4b for $\sigma = 0.30$, even after the peak (in black) a high spike (in blue) can be obtained. However, in Fig. 4c using again $\sigma = 0.30$ and postponing the implementation, a second peak (in blue) without high amplitude is obtained as outcome. Here, the second peak, like the main one, presents around 10 infections (10 per 1000 population). In Fig. 4d applying, after the main peak again, a smaller σ ($\sigma = 0.20$) at the moment for a few numbers of infections, we face the manifestation of a second wave.

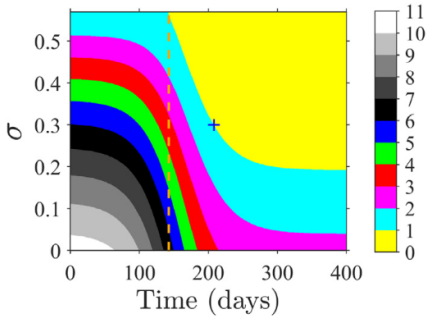

Fig. 5. Two-dimensional diagram of σ *versus* Time (moment) showing the ratio between the new peak value and the flattened curve peak for $\sigma = 0.57$. The golden dashed line indicates the peak for initially applied restriction $\sigma = 0.57$ and the cross in blue corresponds to the response indicated in Fig. 4c. (For interpretation of the references to colour in this figure legend, the reader is referred to the web version of this article.)

In Fig. 5, we investigate the class of cases previously shown in Fig. 4a–d using a two-dimensional diagram in terms of the time (ranging from 0 to 400 days) and the new σ (ranging from 0.40 to 0.57) to simulate easing restrictions. The color is allocated according to the value of the ratio between the new peak value and the flattened curve peak (σ=0.57). The golden dashed line at 142 days indicates the peak for initially applied restriction σ=0.57 and the cross (in blue, in-between yellow and cyan areas) corresponds to the response indicated in Fig. 4c (same amplitude for flattened and second peak curves). Moreover, amplified peaks are obtained for any easing restriction before 142 days (dashed line). For in-

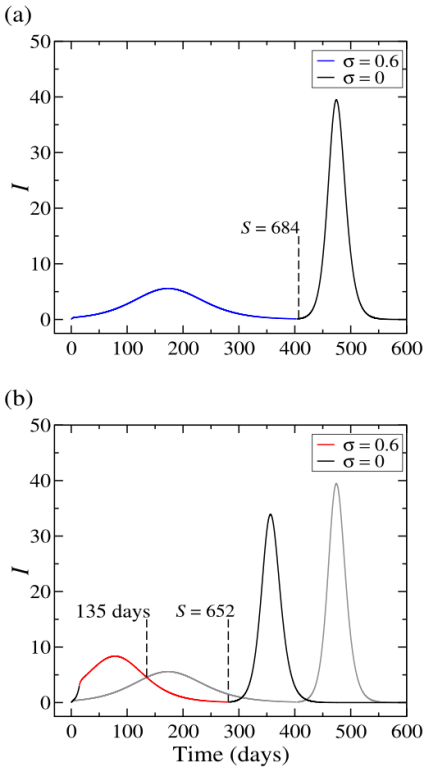

Fig. 6. Time-series of I (infected) showing the effects of the interventions with the appearance of the second wave (black line).

stance, taking σ=0.35 into account the spikes present amplification of peaks between three and five times compared to the flattened curve peak. Even passing the peak (142 days) relaxing restriction can provoke spikes associated with high second peaks, as obtained for σ=0.20 around 200 days with a spreading amplification of twice.

In Fig. 6a and b, we show the effects of the containment measures during the outbreak and the late appearance of the second-wave infections. Fig. 6a displays the epidemic curve (blue line) for $\sigma = 0.6$. When σ is changed to 0, we observe a second wave (black line). Similarly, Fig. 6b displays the infection evolution, but initiating the intervention at two weeks with $\sigma = 0.6$ (red line). As a consequence of delaying containment measures, the number of infections increases considerably in a short time.

We use the two-dimensional diagrams to explore the dynamical properties for the effects shown in Fig. 6a and b. Fig. 7a displays the impact on the amplitude of the first wave in terms of the intensity of intervention σ (ranging from 0 to 0.8) and the number of infections I (initial moment of intervention, ranging from 1 to 100). The amplitude of the first wave is amplified by increasing the delay moment of interventions. Figure 7 b illustrates the effect of the second wave, whose amplitude increases by enlargement of parameter σ applied to the first wave. The red cross corresponds to the curve shown in Fig. 6a with peaks of 5 infections (Fig. 7a, cyan area) and 39 infections (Fig. 7b, light gray area) for the first and second waves, respectively. Moreover, the amplitude of the second wave is associated with the number of susceptibles at the end of the first wave. This effect is verified by comparing Fig. 7c (magnification of Fig. 7b) with Fig. 7d for color allocated according to the effective reproductive numbers ($R_t = R_0 S/N$).

4. Controlling the spread of infections

In the end, we investigate a possible strategy to suppress spikes during easing plan measures. First, considering 10 infected people for the first wave as an acceptable level of infection to prevent collapse in healthcare systems. Such strategy is adopted for just 2 years, based on the assumption that a vaccine or an effective treatment will be available in this period. The interventions are applied at a specific time after the main wave peak and 0.1 infected people moment. Moreover, the new values of parameter σ are evaluated checking the number of susceptible people S and setting $R_t = 1$ for $R_t = R_0(1-\sigma)S/N$.

Fig. 8 a illustrates a case of early response measures for $\sigma = 0.57$ (in black) with the following interventions: first one with $\sigma = 0.51$ (in blue) applied at 30 days after the peak; and the second one with $\sigma = 0.36$ (in red) applied at 0.1 infected people moment. In case of vaccination or effective treatment unavailable in two years, a second wave (in green) appears as a consequence of removing all restrictions. Fig. 8b shows the similar procedure with $\sigma = 0.45$ and $\sigma = 0.37$ for the first, applied at 60 days, and second interventions, respectively. Comparing the results of delaying the intervention from 30 days to 60 days, we evidently obtain a decrease in the intensity of the first intervention (from $\sigma = 0.51$ to $\sigma = 0.45$) and, most importantly, a variation of the susceptible at two years (from $S = 512$ to $S = 525$).

In Fig. 8c, we investigate another case considering the effects of delaying containment measures at the initial stage of the outbreak. To contain the rapid transmission for $\sigma = 0$ (in black), we apply $\sigma = 0.65$ (in light green) at the moment with 7.5 infected people, maintaining the number of infections below 10. The following interventions are given by $\sigma = 0.61$ (at 30 days, in blue) and $\sigma = 0.51$ (in red). The necessary intensive intervention is closely associated with neglecting the outbreak at the initial stage. However, this configuration implies a considerable number of susceptible people, 667, at the end of 2 years. In contrast to the previous case, in Fig. 8d we apply moderate early $\sigma = 0.65$ (the same value of σ used in Fig. 8c) at the moment with 2.5 infected people (instead of 7.5), resulting attenuation of the main peak to (in light green) and significant increase in susceptibles (from 667 to 788) at two years.

Besides preventing spikes during easing measures, the adopted control strategy enables an interesting scenario with a low number of infections (less than 0.1) for a long time (see Fig. 8a–d, lines in red). This scenario is translated into less than 100 infected people for a population of 1 million. A low number of infections facilitates enormously the implementation of public policy responses such as identification, isolation of infected individuals, and efficient contact-tracing approaches [38,39].

Another aspect identified from the control strategy is the variation of the number of susceptibles at two years according to configurations. In fact, the control actuation reshapes the infection curves resulting in this variation. The number of susceptibles is an important outcome, indicating the impact of the disease for the period. In short, increasing susceptible individuals means decreasing the death rate. Fig. 9 shows susceptibles (at two years, the number per 1000) in terms of the moment of first intervention after the peak ($\Delta t = t - t_P$) modeled by $\sigma = 0.57$ since the very beginning (in blue), $\sigma = 0.65$ since 7.5 infected people (in red), and $\sigma = 0.65$ since 2.5 infected people (in green). The pattern of susceptible outcomes is composed of wells following by saturation plateaus. Fig. 10 provides a solid verification of this pattern composition for $\sigma = 0.65$ and I_{bp} as a function of Δt. The color is allocated according to the number of susceptibles at two years. Bearing in mind this quantity the early intervention (before the peak) plays an important role in increasing the susceptibles. Fur-

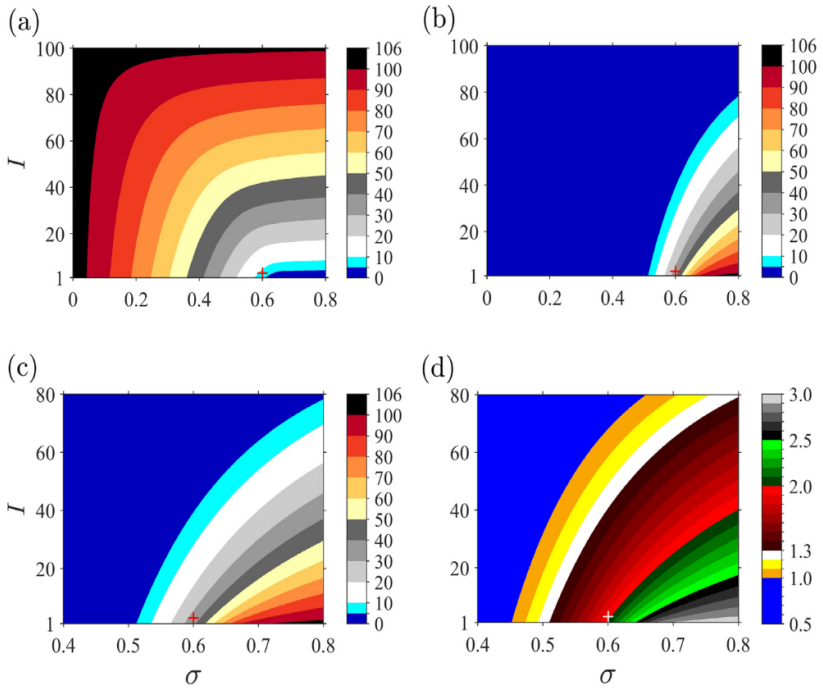

Fig. 7. Two-dimensional diagram of I (number of infections at the moment of intervention) *versus* σ showing (a) the value of the first-wave peak, (b) the value of the second-wave peak for $\sigma = 0$, (c) magnification of previous figure, and (d) the value of the effective reproductive number ($R_t = R_0 S/N$) at the moment of relaxing restriction. The cross corresponds to the curve shown in Fig. 6a.

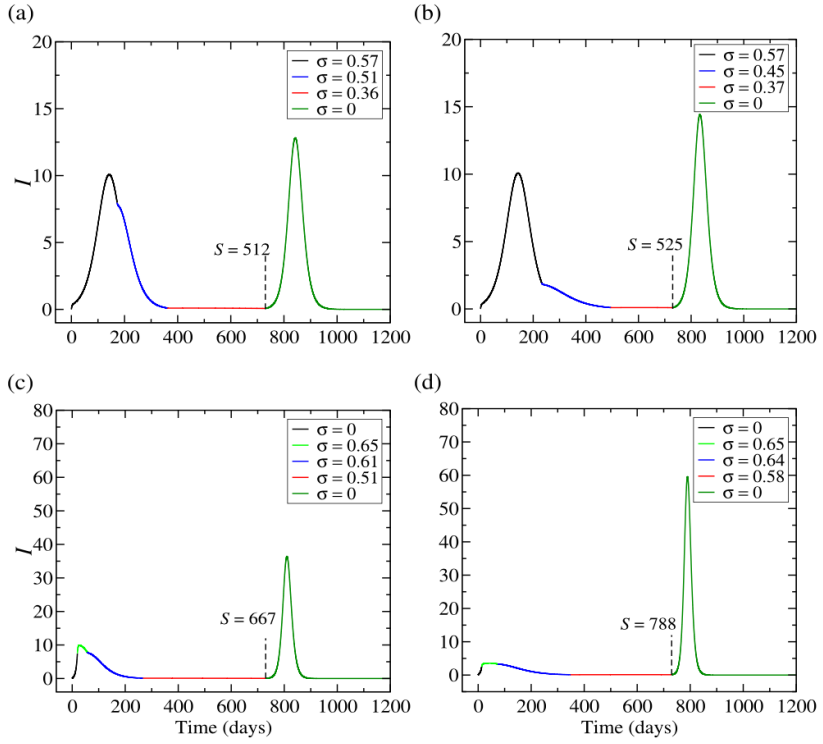

Fig. 8. Time-series of I showing some strategies of controlling infection spread until two years following by second waves (green line). S indicate the number of susceptible people just before of the second wave outbreak. (For interpretation of the references to colour in this figure legend, the reader is referred to the web version of this article.)

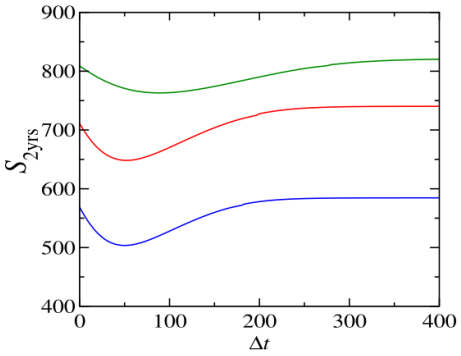

Fig. 9. The number of susceptibles (at two years) as a function of the moment of first intervention after the peak ($\Delta t = t - t_P$) for $\sigma = 0.57$ applied since the very beginning (blue line), $\sigma = 0.65$ since 7.5 infected people (red line), and $\sigma = 0.65$ since 2.5 infected (green line). We consider that births and natural deaths are balanced. (For interpretation of the references to colour in this figure legend, the reader is referred to the web version of this article.)

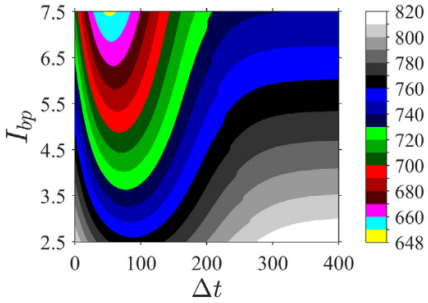

Fig. 10. Two-dimensional diagram showing the number of susceptibles at two years in terms of I_{bp} (moment of the initial intervention using $\sigma = 0.65$) and Δt (the moment of first intervention after the peak). We consider that births and natural deaths are balanced.

thermore, the moment of the first intervention after the peak must also be carefully evaluated to improve the outcomes.

5. Final remarks

To study the infection dynamics of COVID-19 pandemic, we considered the SEIR model with an additional parameter (σ) to simulate the containment restrictions (mitigation measures). Initially, varying σ, we modeled the infection spread obtaining the flatten curves related to all mitigation measures. The curve phenomenon flattening is related to mitigation measures. Additionally, we evaluated the effect of easing restrictions, reducing the value of σ, for the process of reopening the economy and society. In this case, for any easing restrictions applied during increasing infection rates, we obtained high spikes of cases indicating significant acceleration of infections. In general, for the period of decreasing infections, we also obtained prominent spikes describing second-wave of infections.

Finally, we provided a control strategy to suppress spikes during easing restrictions. The interventions are applied at a specific time after the main wave peak and at a moment with low number of infected people. A sequence of control interventions were applied tailoring the parameter sigma during the decreasing infection period. Besides preventing spikes, the analyzed control could contain the transmissibility, for a long time, below 0.1 infections, that means 100 infected people for a population of 1 million. In a practical situation, this low number of infections facilitates enormously the implementation of public health policies such as isolation of infected individuals and contact-tracing.

In this work, we assume that the recovered people can not be infected again. We also consider that the births and natural deaths are balanced, in consequence, the model does not have terms related to the birth and death rates [40]. In future works, we plan to analyse the effects of unbalanced birth and death rates, as well as the possibility of reinfection, in the impact of easing restrictions and control of infection spread.

Declaration of Competing Interest

We wish to confirm that there are no known conflicts of interest associated with this work and there has been no significant financial support for this work that could have influenced its outcome.

CRediT authorship contribution statement

Silvio L.T. de Souza: Conceptualization, Data curation, Formal analysis, Investigation, Methodology, Validation, Visualization, Writing - original draft, Writing - review & editing. **Antonio M. Batista:** Conceptualization, Data curation, Formal analysis, Visualization, Writing - review & editing. **Iberê L. Caldas:** Methodology, Project administration, Resources, Software, Visualization, Writing - review & editing. **Kelly C. Iarosz:** Data curation, Validation, Visualization, Writing - review & editing. **José D. Szezech Jr:** Data curation, Validation, Visualization, Writing - review & editing.

Acknowledgements

This work was possible by partial financial support from the following Brazilian government agencies: CNPq, CAPES, Fundação Araucária, and FAPESP (Grant No. 2015/07311 and 2018/03211-6).

References

[1] McLean A, May R, Pattison J, Weiss R. SARS: a case study in emerging infections. OUP Oxford; 2005.
[2] Anderson RM, Heesterbeek H, Klinkenberg D, Hol-lingsworth TD. How will country-based mitigation measures influence the course of the COVID-19 epidemic? Lancet 2020;395(10228):931–4. doi:10.1016/s0140-6736(20)30567-5.
[3] Anderson R. Population dynamics of infectious diseases. 1st ed. Chapman & Hall; 1982.
[4] Anderson RM, May RM, Anderson B. Infectious diseases of humans: dynamics and control. Oxford University Press; 1992.
[5] Hollingsworth TD. Controlling infectious disease outbreaks: lessons from mathematical modelling. J Public Health Policy 2009;30(3):328–41. doi:10.1057/jphp.2009.13.
[6] Heffernan J, Keeling M. Implications of vaccination and waning immunity. Proc R Soc B 2009;276(1664):2071–80. doi:10.1098/rspb.2009.0057.
[7] Nepomuceno EG, Takahashi RH, Aguirre LA. Reducing vaccination level to eradicate a disease by means of a mixed control with isolation. Biomed Signal Process Control 2018;40:83–90. doi:10.1016/j.bspc.2017.09.004.
[8] Casagrandi R, Bolzoni L, Levin SA, Andreasen V. The SIRC model and influenza A. Math Biosci 2006;200(2):152–69. doi:10.1016/j.mbs.2005.12.029.
[9] Morrison RE, Cunha A Jr. Embedded model discrepancy: a case study of Zika modeling. Chaos 2020;30(5):051103. doi:10.1063/5.0005204.
[10] Weitz JS, Dushoff J. Modeling post-death transmission of ebola: challenges for inference and opportunities for control. Sci Rep 2015;5:8751. doi:10.1038/srep08751.
[11] Lipsitch M, Cohen T, Cooper B, Robins JM, Ma S, James L, Gopalakrishna G, Chew SK, Tan CC, Samore MH, Fisman D, Murray M. Transmission dynamics and control of severe acute respiratory syndrome. Science 2003;300(5627):1966–70. doi:10.1126/science.1086616.
[12] Anderson RM, Fraser C, Ghani AC, Donnelly CA, Riley S, Ferguson NM, et al. Epidemiology, transmission dynamics and control of SARS: the 2002–2003 epidemic. Philos Trans R SocLondon Ser B 2004;359(1447):1091–105. doi:10.1098/rstb.2004.1490.
[13] Lee J, Chowell G, Jung E. A dynamic compartmental model for the Middle East respiratory syndrome outbreak in the Republic of Korea: a retrospective analysis on control interventions and superspreading events. J Theor Biol 2016;408:118–26. doi:10.1016/j.jtbi.2016.08.009.
[14] Ahn I, Heo S, Ji S, Kim KH, Kim T, Lee EJ, et al. Investigation of nonlinear epidemiological models for analyzing and controlling the MERS outbreak in Korea. J Theor Biol 2018;437:17–28. doi:10.1016/j.jtbi.2017.10.004.
[15] Nazarimehr F, Pham V-T, Kapitaniak T. Prediction of bifurcations by varying critical parameters of COVID-19. Nonlinear Dyn 2020. doi:10.1007/s11071-020-05749-6.

[16] Yousefpour A, Jahanshahi H, Bekiros S. Optimal policies for control of the novel coronavirus disease (COVID-19) outbreak. Chaos Solitons Fractals 2020;136:109883. doi:10.1016/j.chaos.2020.109883.

[17] Crokidakis N. COVID-19 spreading in Rio de Janeiro, Brazil: do the policies of social isolation really work? Chaos Solitons Fractals 2020;136:109930. doi:10.1016/j.chaos.2020.109930.

[18] Remuzzi A, Remuzzi G. COVID-19 and Italy: what next? Lancet 2020;395(10231):1225–8. doi:10.1016/s0140-6736(20)30627-9.

[19] Giordano G, Blanchini F, Bruno R, Colaneri P, Filippo AD, Matteo AD, et al. Modelling the COVID-19 epidemic and implementation of population-wide interventions in Italy. Nat Med 2020;26(6):855–60. doi:10.1038/s41591-020-0883-7.

[20] Weitz JS, Beckett SJ, Coenen AR, Demory D, Domin-guez Mirazo M, Dushoff J, et al. Modeling shield immunity to reduce COVID-19 epidemic spread. Nat Med 2020;26(6):849–54. doi:10.1038/s41591-020-0895-3.

[21] Tagliazucchi E, Balenzuela P, Travizano M, Min-dlin GB, Mininni PD. Lessons from being challenged by COVID-19. Chaos Solitons Fractals 2020;137:109923. doi:10.1016/j.chaos.2020.109923.

[22] Duczmal LH, Almeida ACL, Duczmal DB, Alves CRL, Magalhães FCO, de Lima MS, Silva IR, Takahashi RHC. Vertical social distancing policy is ineffective to contain the COVID-19 pandemic. Cadernos de Saúde Pública 2020;36(5):e00084420. doi:10.1590/0102-311x00084420.

[23] Pai C, Bhaskar A, Rawoot V. Investigating the dynamics of COVID-19 pandemic in India under lockdown. Chaos Solitons Fractals 2020;138:109988. doi:10.1016/j.chaos.2020.109988.

[24] Tang B, Bragazzi NL, Li Q, Tang S, Xiao Y, Wu J. An updated estimation of the risk of transmission of the novel coronavirus (2019-nCoV). Infect Dis Modell 2020;5:248–55. doi:10.1016/j.idm.2020.02.001.

[25] Kissler SM, Tedijanto C, Goldstein E, Grad YH, Lipsitch M. Projecting the transmission dynamics of SARS-CoV-2 through the postpandemic period. Science 2020;368(6493):860–8. doi:10.1126/science.abb5793.

[26] Tuite AR, Fisman DN, Greer AL. Mathematical modelling of COVID-19 transmission and mitigation strategies in the population of Ontario, Canada. Can Med Assoc J 2020;192(19):E497–505. doi:10.1503/cmaj.200476.

[27] Wu JT, Leung K, Leung GM. Nowcasting and forecasting the potential domestic and international spread of the 2019-nCoV outbreak originating in Wuhan, China: a modelling study. Lancet 2020;395(10225):689–97. doi:10.1016/s0140-6736(20)30260-9.

[28] Boldog P, Tekeli T, Vizi Z, Dénes A, Bartha FA, Röst G. Risk assessment of novel coronavirus COVID-19 outbreaks outside China. J Clin Med 2020;9(2):571. doi:10.3390/jcm9020571.

[29] Hao X, Cheng S, Wu D, Wu T, Lin X, Wang C. Reconstruction of the full transmission dynamics of COVID-19 in Wuhan. Nature 2020;584:420–4. doi:10.1038/s41586-020-2554-8.

[30] Kucharski AJ, Russell TW, Diamond C, Liu Y, Sun F, Jit M, et al. Early dynamics of transmission and control of COVID-19: a mathematical modelling study. Lancet Infect Dis 2020;20(5):553–8. doi:10.1016/s1473-3099(20)30144-4.

[31] Linka K, Peirlinck M, Kuhl E. The reproduction number of COVID-19 and its correlation with public health interventions. Comput Mech 2020. doi:10.1007/s00466-020-01880-8.

[32] de Souza SLT, Caldas IL. Calculation of Lyapunov exponents in systems with impacts. Chaos Solitons Fractals 2004;19(3):569–79. doi:10.1016/s0960-0779(03)00130-9.

[33] Xu X, Wiercigroch M, Cartmell MP. Rotating orbits of a parametrically-excited pendulum. Chaos Solitons Fractals 2005;23(5):1537–48. doi:10.1016/j.chaos.2004.06.053.

[34] Medeiros ES, de Souza SLT, Medrano-T RO, Caldas IL. Replicate periodic windows in the parameter space of driven oscillators. Chaos Solitons Fractals 2011;44(11):982–9. doi:10.1016/j.chaos.2011.08.002.

[35] de Souza SLT, Lima AA, Caldas IL, Medrano-T RO, Guimarães Filho ZO. Self-similarities of periodic structures for a discrete model of a two-gene system. Phys Lett A 2012;376(15):1290–4. doi:10.1016/j.physleta.2012.02.036.

[36] de Souza SLT, Batista AM, Baptista MS, Caldas IL, Balthazar JM. Characterization in bi-parameter space of a non-ideal oscillator. Physica A 2017;466:224–31. doi:10.1016/j.physa.2016.09.020.

[37] Rech PC. Organization of the periodicity in the parameter-space of a glycolysis discrete-time mathematical model. J Math Chem 2018;57(2):632–7. doi:10.1007/s10910-018-0976-4.

[38] Kwok KO, Tang A, Wei VW, Park WH, Yeoh EK, Riley S. Epidemic models of contact tracing: systematic review of transmission studies of severe acute respiratory syndrome and middle east respiratory syndrome. Comput Struct Biotechnol J 2019;17:186–94. doi:10.1016/j.csbj.2019.01.003.

[39] Sinha P, Paterson AE. Contact tracing: can 'big tech' come to the rescue, and if so, at what cost? EClinicalMedicine 2020:100412. doi:10.1016/j.eclinm.2020.100412.

[40] Carcione JM, Santos JE, Bagaini C, Ba J. A simulation of a COVID-19 epidemic based on a deterministic SEIR model. Front Public Health 2020:230. doi:10.3389/fpubh.2020.00230.